

# Alteration of Sediments by Hyperalkaline K-Rich Cement Leachate: Implications for Strontium Adsorption and Incorporation

Sarah H. Wallace,<sup>†</sup> Samuel Shaw,<sup>†,‡</sup> Katherine Morris,<sup>‡</sup> Joe S. Small,<sup>§</sup> and Ian T. Burke<sup>\*,†</sup>

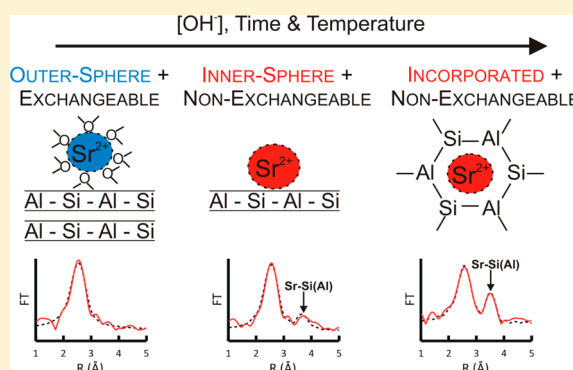
<sup>†</sup>Earth Surface Science Institute, School of Earth and Environment, University of Leeds, Leeds, LS2 9JT, United Kingdom

<sup>‡</sup>Research Centre for Radwaste and Decommissioning and Williamson Research Centre, School of Earth, Atmospheric and Environmental Sciences, University of Manchester, Manchester, M13 9PL, United Kingdom

<sup>§</sup>National Nuclear Laboratory, Risley, Warrington, Cheshire, WA3 6AE, United Kingdom

## Supporting Information

**ABSTRACT:** Results are presented from 1 year batch experiments where K-rich hyperalkaline pH 13.5 young cement water (YCW) was reacted with sediments to investigate the effect of high pH, mineral alteration, and secondary mineral precipitation on <sup>90</sup>Sr sorption. After reaction with YCW, Sr sorption was found to be greater than 75% in all samples up to 365 days and 98% in a sample reacted for 365 days at 70 °C. Scanning electron microscopy analysis of sediment samples reacted at room temperature showed surface alteration and precipitation of a secondary phase, likely a K-rich aluminosilicate gel. The presence of Sr–Si(Al) bond distances in Sr K-edge extended X-ray absorption fine structure (EXAFS) analysis suggested that the Sr was present as an inner-sphere adsorption complex. However, sequential extractions found the majority of this Sr was still exchangeable with Mg<sup>2+</sup> at pH 7. For the sample reacted for 1 year at 70 °C, EXAFS analysis revealed clear evidence for ~6 Sr–Si(Al) backscatters at 3.45 Å, consistent with Sr incorporation into the neoformed K-chabazite phase that was detected by X-ray diffraction and electron microscopy. Once incorporated into chabazite, <sup>90</sup>Sr was not exchangeable with Mg<sup>2+</sup>, and chemical leaching with pH 1.5 HNO<sub>3</sub> was required to remobilize 60% of the <sup>90</sup>Sr. These results indicate that, in high pH cementitious leachate, there is significantly enhanced Sr retention in sediments due to changes in the adsorption mechanism and incorporation into secondary silicate minerals. This suggests that Sr retention may be enhanced in this high pH zone and that the incorporation process may lead to irreversible exchange of the contaminant over extended time periods.



## INTRODUCTION

The use of cementitious materials is ubiquitous at nuclear facilities around the world, where it is utilized in buildings, storage facilities, and also the packaging of radioactive waste. When fresh cement and concrete come into contact with water, a highly alkaline (0.3–0.7 mol L<sup>-1</sup> OH<sup>-</sup>) K- and Na-rich fluid forms, commonly known as young cement water (YCW).<sup>1</sup> Interaction of such a hyperalkaline solution with aluminosilicate minerals in natural soils (e.g., clay minerals) and rock promotes the dissolution and recrystallization of these minerals to neoformed phases (e.g., zeolites).<sup>2–9</sup> These reactions lead to the formation of an alkaline disturbed zone in the geosphere surrounding the cement structures, which significantly alters the chemical (e.g., adsorption capacity) and physical (e.g., porosity) properties of the soils or sediment. In turn, this could affect the mobility and speciation of radionuclides accidentally released into these environments. Therefore, understanding the processes occurring at the cement–geosphere interface and the effect of alkaline alteration on radionuclide speciation and mobility is key to the safe decommissioning of nuclear sites, some of which are considered the most hazardous facilities on the planet.<sup>10</sup>

It is generally accepted that the reaction of aluminosilicate clay minerals (such as those found in bentonite) with alkaline fluids follows a two-stage process: initial dissolution that releases Si and Al into solution followed by precipitation/recrystallization of newly formed phases.<sup>3</sup> The exact reaction pathway and end product formed are highly dependent on the primary mineral (composition and structure), fluid composition, and temperature.<sup>4,11–14</sup> Studies of cement leachate interaction with bentonite barrier materials, which will be used in several national geodisposal repository programs,<sup>1,8,9,15</sup> indicates that these reactions lead to the formation of zeolites and/or calcium (aluminum) silicate hydrate (C–S–H) phases as reaction end points. Such phases have also been observed to occur at natural analogue sites where natural alkaline fluids (pH 12–13) react with silicate minerals in rocks.<sup>16,17</sup> Studies of the mechanism of these secondary phase formation reactions from clays (e.g., kaolinite and bentonite), mixed with Na-rich fluids

Received: December 19, 2012

Revised: March 15, 2013

Accepted: March 19, 2013

Published: March 19, 2013

in model systems, show that the reaction proceeds via amorphous aluminosilicate and zeolite intermediate phases<sup>12</sup> with complete transformation to sodalite ( $\text{Na}_8\text{Cl}_2[\text{Al}_6\text{Si}_6\text{O}_{24}]$ ) and cancrinite ( $\text{Na}_6\text{Ca}_2[(\text{CO}_3)_2][\text{Al}_6\text{Si}_6\text{O}_{24}]\cdot 2\text{H}_2\text{O}$ ) phases at elevated temperatures or after very long reaction times.<sup>12</sup> However, the reaction of highly alkaline K-rich cement leachates with natural sediments/soils relevant to nuclear contaminated land and the alteration pathways of clay minerals in these systems have not been widely investigated.

Previous research of alkaline alteration of vadose zone sediments has focused on the interaction with highly caustic leak solutions, containing elevated concentrations of  $\text{Na}^+$ ,  $\text{NO}_3^-$ , and  $\text{Al}^{3+}$ , relevant to the U.S. Department of Energy Hanford site.<sup>2,3,18–20</sup> Experimental studies conducted at a variety of temperatures have shown the formation of a wide range of secondary phases including zeolites, cancrinite, and sodalite.<sup>21</sup> These minerals have framework structures with channels and cages that can accommodate both cations and anions.<sup>4</sup> Indeed, it has been demonstrated that both  $\text{Sr}^{2+}$  and  $\text{Cs}^+$  can readily substitute into cancrinite and sodalite during alkaline alteration and once incorporated are relatively resistant to further remobilisation.<sup>19,22</sup> Therefore, it has been proposed that this mechanism could be exploited for the retardation of contaminant radionuclides such as  $^{90}\text{Sr}$  and  $^{137}\text{Cs}$  under alkaline conditions.<sup>23</sup> However, the composition of cement leachate (i.e., dominated by  $\text{K}^+$ ,  $\text{Na}^+$ , and  $\text{Ca}^{2+}$ ) is different to Hanford tank compositions, and therefore, a different reaction pathway may be expected. Clearly, this is highly relevant to some legacy sites where accidentally released  $^{90}\text{Sr}$ -bearing fluids will have passed through and reacted with cementitious materials, prior to release into the surface soils and sediments.

Therefore, this study had the following objectives: (1) investigate the nature of the mineral alteration reactions produced by highly alkaline cementitious leachate in contact with chlorite containing sediments (relevant to the U.K. Sellafield nuclear site) during incubation over long time scales (1 year); (2) use X-ray absorption spectroscopy (XAS) to determine the nature of  $\text{Sr}^{2+}$  incorporation occurring within secondary mineral precipitates and sequential extractions to assess exchangeability and potential mobility of  $\text{Sr}^{2+}$  associated with these phases; (3) use the data produced to infer the likely importance of alkaline alteration of sediments in cementitious environments with respect to radionuclide mobility.

## MATERIALS AND METHODS

**Sediment Collection and Characterization.** Unconsolidated sediments representative of the Sellafield nuclear facility in North West England were collected in August 2009 (lat  $54^\circ 26.3' \text{ N}$ , long  $3^\circ 28.2' \text{ W}$ ). The sediment was dried at  $40^\circ \text{C}$  and sieved to retain the less than 2 mm fraction. Sediment characteristics are described in refs 24–26. Briefly, the sediment was a fine grained silty sand ( $3 \pm 1\%$  clay). The mineralogy was dominated by quartz ( $\text{SiO}_2$ ) and feldspars (e.g., (K, Na)- $\text{AlSi}_3\text{O}_8$ ). Chlorite ( $\text{Mg}_3\text{Al}(\text{AlSi}_3\text{O}_{10}(\text{OH})_8)$ ) was the dominant clay mineral with minor amounts of illite ((K,  $\text{H}_3\text{O}$ )(Al, Mg, Fe) $_2(\text{Si}, \text{Al})_4\text{O}_{10}(\text{OH})_2$ ) also detected. The sediment contained  $\sim 0.5\%$  organic carbon. Scanning electron microscopy (SEM) analysis revealed that the sediment contained angular and subangular quartz, feldspar, and silicate rock fragments (mean grain size = 0.25 mm) coated in fine grained clay and iron oxide particles. The natural Sr content was  $56 \text{ mg kg}^{-1}$ , which was nonexchangeably associated with minerals.

**Batch Sorption Experiments.** YCW (pH 13.5) was made as follows: 25 mL of saturated  $\text{Ca}(\text{OH})_2$  solution, 2.173 g of  $\text{Na}_2\text{SO}_4$ , 2.876 g of NaOH, and 19.86 g of KOH in 1 L of deoxygenated DIW (saturated  $\text{Ca}(\text{OH})_2$  solution was made by placing 20 g of  $\text{Ca}(\text{OH})_2$  in a dialysis bag and equilibrated for 120 days in 1 L of deoxygenated DIW; pH 12.7). Dried sediment was weighed into 50 mL polypropylene Oak Ridge tubes and mixed with the YCW solution containing  $20 \text{ mg L}^{-1}$   $\text{Sr}^{2+}$  (as  $\text{SrCl}_2$ ) at a solid/solution ratio of  $20 \text{ g L}^{-1}$ , in an anaerobic chamber (97%  $\text{N}_2/3\% \text{ H}_2$ ; Coy Ltd., CA). All tubes were stored, in the dark, at  $21^\circ \text{C}$ , inside airtight jars containing Carbosorb to remove atmospheric  $\text{CO}_2$  for up to a year (carbonate would not form in the center of an alkaline subsurface plume; therefore,  $\text{CO}_2$  was excluded to avoid carbonate formation in experiments). Triplicate tubes were sacrificed at 2, 10, 30, 90, 180, and 365 days. One set of triplicate tubes was stored in the dark at  $70^\circ \text{C}$  for 1 year (hereafter referred to as “365 days +70 °C”). In addition, a duplicate set of three tubes for each time point was spiked with  $30 \text{ Bq mL}^{-1}$   $^{90}\text{Sr}$  tracer ( $6.5 \times 10^{-11} \text{ mol L}^{-1}$  as  $\text{SrCl}_2$  in  $0.01 \text{ mol L}^{-1}$  HCl; CERCA-LEA, France) under argon, for aqueous geochemistry and sequential extraction measurements. At each sampling point, tubes were centrifuged at  $6000g$  for 10 min, and the supernatant removed. The pH was determined in the aqueous phase using an Orion benchtop meter, and major element concentrations were determined on a Perkin–Elmer 5300DV inductively coupled plasma optical emission spectrometer (ICP-OES). Moist sediments from nonactive tubes were stored at  $-80^\circ \text{C}$  prior to XAS analysis. Mineralogical components and the physical characteristics of the sediments were determined by X-ray diffraction (XRD), Brunauer–Emmett–Teller (BET), and electron microscopy (see Section 1 of the Supporting Information for details).

**Sequential Extractions.** Sequential extractions were carried out on tubes containing  $^{90}\text{Sr}$  at each time point following an adapted Tessier/BCR method<sup>27,28</sup> (see Table S1 of the Supporting Information for further details). The tubes were spun at  $6000g$  for 10 min, and the porewater was removed and filtered ( $0.2 \mu\text{m}$ ). The sediment was then progressively leached with  $1 \text{ mol L}^{-1}$   $\text{MgCl}_2$  (pH 7, 2 h),  $1 \text{ mol L}^{-1}$  sodium acetate (pH 5, 5 h), and finally,  $0.5 \text{ mol L}^{-1}$  acidic hydroxylammonium chloride (pH 1.5, 12 h). Between each stage, the tubes were centrifuged, the supernatant was removed and filtered as before, and 1 mL of each extraction leachate was analyzed for  $^{90}\text{Sr}$  by liquid scintillation counting (LSC) on a Parkard Tri-Carb 2100TR (see Section 2 of the Supporting Information for details).

**XAS.** Sr K-edge (16 105 eV) XAS spectra were collected at beamline BM26A at the European Synchrotron Radiation Facility in January 2011. Approximately 300 mg of moist sediment samples (10 days, 365 days, and 365 days +70 °C) were prepared under argon atmosphere in aluminum holders with Kapton windows, and data were collected at 80 K using a liquid nitrogen cryostat. Spectra were also collected from a  $\text{SrCl}_2$  solution ( $3000 \text{ mg L}^{-1}$ ) and  $\text{SrCO}_3$  standards. Extended X-ray absorption fine edge structure (EXAFS) spectra were averaged using Athena v0.8.061, and the background was subtracted using PySpline v1.1.<sup>29</sup> EXAFS data were analyzed in DLexcurv v1.0<sup>30</sup> using full curved wave theory.<sup>31</sup> The data were fitted for each sample by defining a theoretical model and comparing the calculated EXAFS spectrum with experimental data. Shells of backscatterers were added around the Sr and by refining an energy correction  $E_f$  (the Fermi energy), the

absorber–scatterer distance, and the Debye–Waller factor for each shell; a least-squares residual (the  $R$  factor<sup>32</sup>) was minimized. Shells or groups of shells were only included if the overall fit ( $R$  factor) was reduced by greater than 5% (see ref 33 and Section S3 of the Supporting Information for further details of beamline setup and analysis protocols).

## RESULTS

**Solution Analysis and Sequential Extractions.** During reaction of the sediment with YCW, the pH remained at  $13.49 \pm 0.29$  in all experiments. The activity of the  $^{90}\text{Sr}$  tracer in solution (aqueous phase in Figure 1) decreased from 30 Bq

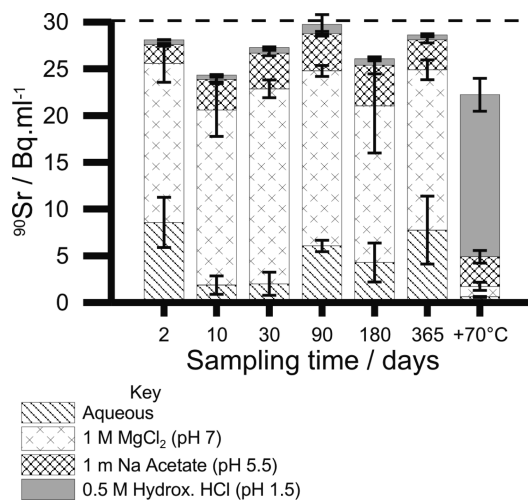


**Figure 1.**  $^{90}\text{Sr}$  concentrations recovered in sequential extractions performed on sediments aged in YCW solution. Dashed line at 30 Bq  $\text{mL}^{-1}$  equates to 100% recovery.

$\text{mL}^{-1}$  at the start of the 21 °C reaction to  $8.6 \pm 2.7$  Bq  $\text{mL}^{-1}$  after 2 days, decreasing to a minimum of  $1.9 \pm 1.0$  Bq  $\text{mL}^{-1}$  after 10 days. During further aging, the  $^{90}\text{Sr}$  activity in solution gradually rose to reach  $7.7 \pm 3.6$  Bq  $\text{mL}^{-1}$  at 365 days. In sequential extractions, the majority (70–80%) of the  $^{90}\text{Sr}$  activity associated with sediment was recovered in the  $\text{MgCl}_2$  exchangeable fraction, with the remaining 20–30% recovered in other fractions or residual. In the 365 days +70 °C sample, only  $0.6 \pm 0.1$  Bq  $\text{mL}^{-1}$  was found in solution with the majority ( $17.3 \pm 1.8$  Bq  $\text{mL}^{-1}$ ; 60.2 ± 6.2%) of the  $^{90}\text{Sr}$  added recovered in the acidic hydroxylammonium chloride fraction, and 24 ± 6% was residual.

At 2 days, the Si and Al concentrations ( $714 \pm 229$  and  $22 \pm 8$  mg  $\text{L}^{-1}$ , respectively) are elevated despite neither being added to the initial YCW composition (Figure 2). Thereafter, the Si and Al concentrations decrease at day 10, then remain at broadly similar levels from 10 to 365 days with an initial decrease to minimum concentrations of  $16 \pm 1$  and  $11 \pm 1$  mg  $\text{L}^{-1}$ , respectively, at 30 days, and then, a slow increase to  $45 \pm 10$  and  $43 \pm 8$  mg  $\text{L}^{-1}$ , respectively, by 365 days. In the 365 days +70 °C sample, the Si concentration is  $949 \pm 115$  mg  $\text{L}^{-1}$ , and the Al concentration is  $2.6 \pm 0.1$  mg  $\text{L}^{-1}$ . Aqueous K and Na concentrations at 2 days were slightly below YCW composition, the K concentration was  $11\,600 \pm 700$  mg  $\text{L}^{-1}$ , and the Na concentration was  $2000 \pm 100$  mg  $\text{L}^{-1}$  (vs  $13\,833 \pm 1100$  and  $2350 \pm 190$  mg  $\text{L}^{-1}$  in YCW). K and Na concentrations reached minimum values of  $5800 \pm 300$  and  $1100 \pm 20$  mg  $\text{L}^{-1}$ , respectively, at 30 days. K and Na

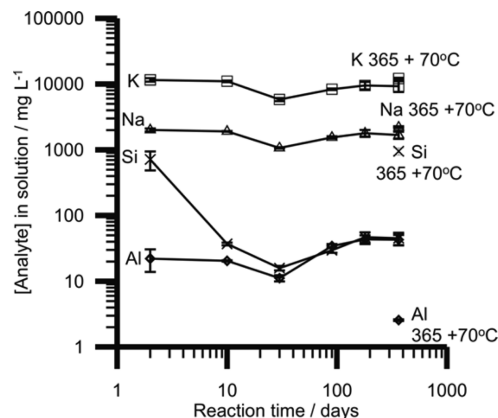


**Figure 2.** Concentration of selected major elements during the 1 year reaction of sediments with YCW.

concentrations then steadily increased to within error of the concentration reported from the 2 day sample in both the 365 days and the 365 days +70 °C samples.

**XRD, SEM, BET, and Electron Microprobe Analyses.** XRD results (Figure 3) indicated that the bulk mineralogy of

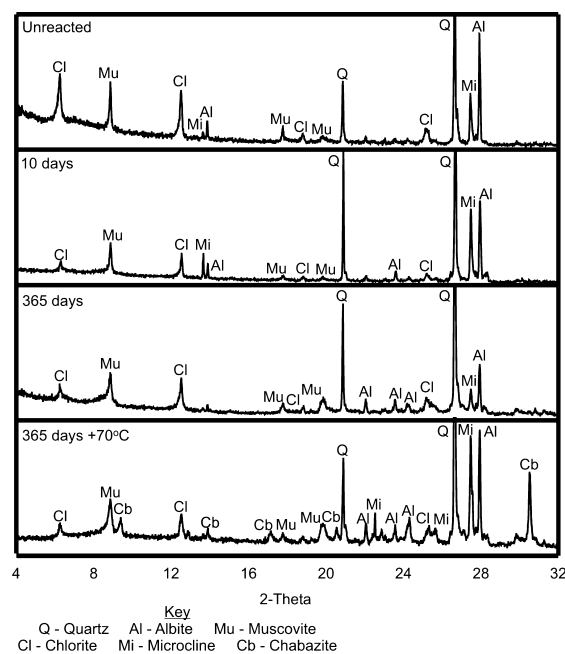


**Figure 3.** XRD patterns collected from fine fraction sediment samples at time points shown. Chlorite peaks are relatively more prominent in unreacted sediments; chabazite peaks are only found for the sample incubated for 365 days at 70 °C.

the sediments did not change during the reaction with YCW up to 365 days. However, qualitatively, the intensity of the chlorite peaks relative to the peaks of the bulk mineral phases (i.e., quartz and feldspar) was reduced in samples reacted with YCW compared to unreacted sediments, whereas the illite/muscovite peaks were unchanged. SEM analysis of the unreacted sediment (Figure 4a) revealed sand- and silt-sized quartz and feldspar grains coated with less than 5  $\mu\text{m}$  of aluminosilicate clay particles with a platelike morphology. After 10 days of reaction with YCW (Figure 4b), the clay particles were still visible as a surface coating on the grains, but their surface appeared altered, that is, smoother. Energy dispersive X-ray (EDX) analyses of

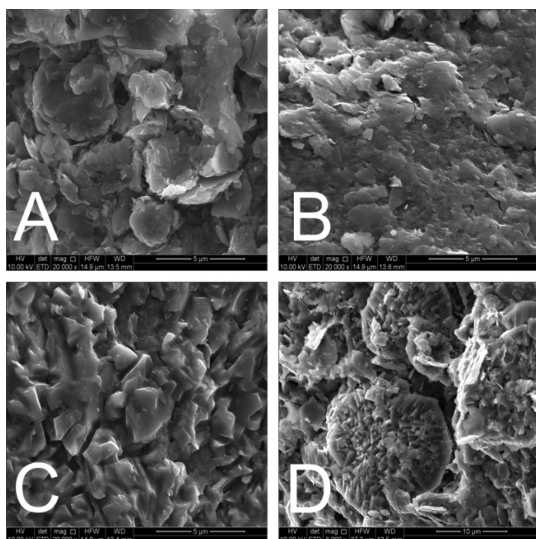


**Figure 4.** Scanning electron photomicrographs of sediment samples under the following conditions: (A) unreacted coarse sediment; (B) after 10 days of reaction in YCW; (C) after 365 days of reaction in YCW; and (D) after 365 days of reaction at 70 °C.

the aluminosilicate clay particles (Figure S1, Supporting Information) showed they contained elevated K compared to the material coating the unreacted sediments. After 365 days of reaction (Figure 4c), the surfaces of the grains were coated with a smooth fine grained (i.e., nanoparticulate) secondary precipitate. EDX analyses revealed the precipitate had a similar K-rich aluminosilicate composition as was present at 10 days. Due to the thinness of the coating, the presence of other phases in the EDX excitation volume ( $\sim 2 \mu\text{m}^3$ ) could not be excluded; therefore, it was impossible to determine a reproducible EDX analysis of the coating.

In the 365 days +70 °C sample additional peaks were present in XRD patterns that were assigned to the zeolite mineral, chabazite. In contrast to sediments from reactions at room temperature, sediment grains in the 365 days +70 °C sample (Figure 4d) were coated in flattened 5–10  $\mu\text{m}$  diameter disc-shaped crystals made up of smaller intergrown crystallites. This morphology is similar to previous reports of newly formed chabazite.<sup>5</sup> SEM-EDX analysis of the new phases consisted of K–Na–Al–Si–O (Figure S1, Supporting Information). Electron microprobe analysis of the individual particles (Figure S2 and Table S2, Supporting Information) yielded a chemical formula of  $(\text{K}_{1.2}\text{Na}_{0.3}\text{Sr}_{0.1}\text{Ca}_{0.1})[\text{Si}_{2.5}\text{Al}_{3.6}\text{O}_{12}]\cdot 5.9\text{H}_2\text{O}$  (Table S3, Supporting Information) consistent with the idealized formula of K-chabazite,  $(\text{K}_2\text{Al}_2\text{Si}_4\text{O}_{12})\cdot 6\text{H}_2\text{O}$  substituted with  $\sim 2 \pm 1$  wt % Sr. The BET surface area of the unreacted sediment was measured as  $4.69 \pm 0.01 \text{ m}^2 \text{ g}^{-1}$ . After 10 days of reaction, the surface area measured in the sample had decreased to  $1.46 \pm 0.02 \text{ m}^2 \text{ g}^{-1}$  (Table 1). Further time points in the experiments at 21 °C showed no significant change in surface area. In contrast, in the 365 days +70 °C sample, the surface area was  $5.45 \pm 0.03 \text{ m}^2 \text{ g}^{-1}$ .

**Sr EXAFS Analysis.** Sr K-edge EXAFS data collected from sediment reacted with YCW for 10 days (Figure 5; Table 2) revealed a Sr coordination environment of  $\sim 8$  O atoms at 2.59 Å. Data was fitted with one further shell containing  $\sim 3$  Si(Al) backscatters at 3.79 Å (due to their similar atomic mass, Si and Al are indistinguishable in EXAFS analysis). Data collected from the sample recovered after 365 days of reaction also

**Table 1.** BET Surface Area Measured in Sediments Reacted in YCW

sample	BET surface area ( $\text{m}^2 \text{ g}^{-1}$ )
unreacted	$4.69 \pm 0.01$
10 days	$1.46 \pm 0.02$
30 days	$2.11 \pm 0.31$
90 days	$1.49 \pm 0.01$
180 days	$1.37 \pm 0.01$
365 days	$1.66 \pm 0.02$
365 days +70 °C	$5.45 \pm 0.03$

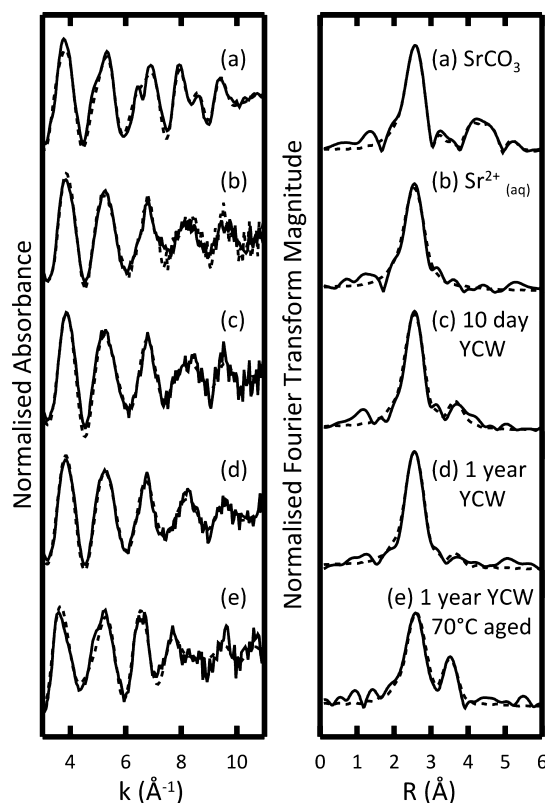


**Figure 5.** Background subtracted Sr K-edge EXAFS spectra (left-hand side) and related Fourier transformations (right-hand side) collected from (a)  $\text{SrCO}_3$ , (b)  $3000 \text{ mg L}^{-1} \text{ Sr}^{2+}$  solution, and (c–e) sediment samples aged with  $\text{Sr}^{2+}$  and YCW for 10 days, 365 days, or 365 days at 70 °C. Dashed lines represent model fits produced in DLExcurv V1.0 using the parameters listed in Table 2.

revealed a first shell coordination of  $\sim 8$  O atoms at 2.60 Å and a second shell fitted with  $\sim 1$  Si(Al) backscatter at 3.84 Å. In the 365 days +70 °C sample, the EXAFS data was best fit with a first shell containing  $\sim 8$  O atoms at 2.67 Å and a single additional shell of  $\sim 6$  Si(Al) backscatters at 3.45 Å.

## DISCUSSION

**Low-Temperature (21 °C) Reaction of Sediments with YCW.** Addition of alkaline fluids, such as K-rich YCW, to sediments induces a rapid (within 2 days) initial dissolution of the reactive, high surface area aluminosilicate clay within the sediment leading to a rapid increase in dissolved Si and Al.<sup>18</sup> Consistent with previous observations of alkaline sediment alteration,<sup>21</sup> in these experiments, XRD analysis suggests that chlorite appears to be the key reactive clay phase within the sediment. After 10 days of reaction at room temperature, the observed surface alteration of the sediment grains, in

**Table 2. Sr K-edge EXAFS Model Fitting Parameters Where  $n$  Is the Occupancy ( $\pm 25\%$ ),  $r$  Is the Interatomic Distance ( $\pm 0.02$  Å for the First Shell,  $\pm 0.05$  Å for Outer Shells),  $2\sigma^2$  Is the Debye–Waller Factor ( $\pm 25\%$ ), and  $R$  Is the Least Squares Residual**

sample	shell	$n$	$r$ (Å)	$2\sigma^2$ (Å <sup>2</sup> )	$R$	
Sr <sup>2+</sup> solution	O	9.1	2.58	0.031	26.3	
	SrCO <sub>3</sub>	O	9 <sup>a</sup>	2.64	0.027	20.3
		C	6 <sup>a</sup>	3.04	0.032	
		Sr	6 <sup>a</sup>	4.22	0.029	
YCW 10 days	Sr	4 <sup>a</sup>	4.97	0.033		
	O	8.5	2.59	0.025	27.3	
YCW 365 days	Si(Al)	2.7	3.79	0.020		
	O	7.8	2.60	0.024	21.8	
YCW 365 days +70 °C	Si(Al)	1.2	3.84	0.018		
	O	8.2	2.67	0.027	32.9	
	Si(Al)	5.5	3.45	0.028		

<sup>a</sup>Fixed.

conjunction with the rapid increase then decline in Si and Al solution concentration, indicated that precipitation of a secondary phase had begun to occur (as observed in similar alkaline alteration experiments using Hanford sediments<sup>34</sup>). The K–Al–Si-rich composition of this coating, lack of defined crystalline morphology, and XRD peaks indicates it is either a K-rich aluminosilicate amorphous gel or nanocrystalline phases where the crystalline particles are too small to form distinct XRD peaks. However, at the temperature and duration of the experiments, the formation of an amorphous gel is most plausible.<sup>5</sup>

By 365 days of reaction at room temperature, SEM indicated a large increase in the amount of the secondary aluminosilicate phase formed. Again, the lack of any crystalline morphology and the absence of any additional peaks in the XRD pattern of the reaction products suggest the secondary phases has remained poorly ordered. A small increase in  $SSA_{BET}$  was observed ( $1.46 \pm 0.02$  to  $1.66 \pm 0.01$  m<sup>2</sup> g<sup>-1</sup>) after 365 days of reaction and was also attributed to the presence of increased amounts of the secondary phase. SEM-EDX analysis of the secondary phase at 365 days showed that it remained a K-rich aluminosilicate gel. This is consistent with other studies that show the formation of aluminosilicate gels from Si- and Al-rich solutions.<sup>5,34</sup> Alkaline alteration of aluminosilicates commonly proceeds via dissolution and precipitation of amorphous gel phases that can then transform to more crystalline phases with time and temperature.<sup>7,12</sup> At 21 °C, however, the temperature was presumably too low to allow crystallization.

The majority of the <sup>90</sup>Sr tracer added remained sorbed (“sorbed” or “sorption” here refers to Sr removed from solution with no specific information regarding whether it is surface adsorbed or incorporated) to sediments throughout the 365 days of reaction with YCW (pH = 13.5) at room temperature ( $K_d = 180$  and  $700$  L kg<sup>-1</sup> at 365 and 10 days, respectively). This is in contrast to previous work using the same sediment,<sup>26</sup> which showed that Sr adsorption decreases with pH above 8 due to the increase in ionic strength caused by the addition of Na<sup>+</sup> or Ca<sup>2+</sup> ions and cation exchange of the outer-sphere adsorbed Sr (“adsorbed” or “adsorption” here refers to Sr specifically associated with mineral surfaces). At a pH of 10, the adsorption of <sup>90</sup>Sr was low ( $K_d \sim 1$  L kg<sup>-1</sup>), and if this trend were to continue, it predicts that, at pH 13.5, <sup>90</sup>Sr adsorption would be extremely low due to high ionic strength (>0.1 mol

L<sup>-1</sup> in YCW). Interestingly, our data contradicts this prediction indicating that Sr is sorbed to the mineral particles via a different mechanism than that at lower pH (e.g., pH ≤ 10). Sr K-edge EXAFS spectra collected from samples recovered at 10 and 365 days (Figure 5) did not indicate that the Sr was present as a simple outer-sphere adsorption complex, due to the presence of Si(Al) atoms at bond distance  $\approx 3.8$  Å. This is consistent with Sr–Si(Al) bond distances observed in previous alkaline alteration experiments using natural sediments that were attributed to inner-sphere adsorption to secondary aluminosilicate phases.<sup>19</sup> Therefore, we suggest that the high levels of sorption at pH 13.5 observed in these experiments was due to inner-sphere adsorption of Sr associated with the secondary K-rich aluminosilicate precipitate or altered clay minerals (Figure 4d).

This interpretation explains the large difference in adsorption observed at pH 10<sup>26</sup> relative to pH 13.5 in this study, as our data suggest there is a fundamental change in the adsorption mechanism that then dramatically increases adsorption. This is because, unlike outer-sphere adsorption, surface uptake during inner-sphere adsorption is not affected by ionic strength.<sup>35</sup> However, it should be noted that, in our experiments, a high proportion of the <sup>90</sup>Sr was exchanged from the sediments using a pH 7 MgCl<sub>2</sub> extraction. The apparent selectivity of Sr<sup>2+</sup> to exchange with Mg<sup>2+</sup> rather than Na<sup>+</sup> or K<sup>+</sup> in the YCW solution was attributed to a change in adsorption mechanism when the alkaline reacted materials were reacted with a pH 7, 1 mol L<sup>-1</sup> MgCl<sub>2</sub> solution. The direct addition of the solution to reacted sediments resulted in a substantial decrease in pH, changing the Sr adsorption to an outer-sphere mechanism that is susceptible to exchange by Mg<sup>2+</sup>. We suggest that this observation shows that the change in Sr adsorption mechanism is not due to the alteration of the silicate minerals by the alkaline fluid but is simply a function of the high pH.

**High-Temperature (70 °C) Reaction of Sediments with YCW.** Reaction of the sediment with K-rich YCW for 365 days at 70 °C produced a new crystalline phase. A combination of morphological, XRD, and microprobe data provides strong evidence that K-chabazite (zeolite) was the stable end point of alkaline alteration. The formation of K-chabazite has also been observed in reactions of bentonite and KOH-dominated alkaline solutions at similar pH and temperature (pH 13.5, 60 °C).<sup>5</sup> The crystalline end-product formed is often controlled by the composition of the alkaline fluid. For example, the reaction of bentonite with NaOH solution (pH > 12.9), produces Na-rich analcime (NaAlSi<sub>2</sub>O<sub>6</sub>·H<sub>2</sub>O),<sup>15</sup> whereas alteration of sediments with Na-, Al-, and nitrate-rich fluids (pH > 13) (such as those found at the U.S. Hanford site) more commonly forms feldspathoids such as sodalite and cancrinite.<sup>19,36</sup>

In the 365 days +70 °C sample, very high <sup>90</sup>Sr  $K_d$  values were observed ( $\sim 2500$  L kg<sup>-1</sup>) indicating that formation of chabazite promoted much higher levels of Sr sorption than the room-temperature reaction. Sr K-edge EXAFS spectra collected from reference chabazite show a characteristic elongated first shell Sr–O bond distance at 2.67 Å (compared to a more usual Sr–O distance of  $\sim 2.60$  Å found where Sr is present in a hydration sphere) and strong second shell Sr–Si(Al) scattering at 3.45 Å.<sup>21</sup> The EXAFS spectra collected from the 365 days +70 °C sample had a similar elongation of the first shell Sr–O bond distance (2.67 Å) and also featured a strong second shell of  $\sim 6$  Sr–Si(Al) backscatterers at a distance of 3.45 Å, consistent with incorporation of Sr into the

neofomed chabazite. These bond distances are correct for incorporation of  $\text{Sr}^{2+}$  into the aluminosilicate cage within the chabazite structure below the D6R ring (cation site 1 in ref 37). Sequential extraction results demonstrated that  $^{90}\text{Sr}$  incorporated in this site is nonexchangeable with  $\text{Mg}^{2+}$ , primarily due to the small diameter cage entrance compared with the hydrated  $\text{Sr}^{2+}$  ionic radius ( $\sim 3.8$  Å for the cage entrance vs  $\sim 5.2$  Å for hydrated  $\text{Sr}^{2+}$ ).<sup>38–40</sup> Once incorporated,  $\text{Sr}^{2+}$  is therefore recalcitrant to extraction by ion exchange, and rerelease requires dissolution of the hosting mineral.<sup>19,22</sup> Our sequential extraction results showed the majority of the  $^{90}\text{Sr}$  tracer was recovered during acidic hydroxylammonium chloride (pH 1.5) leaching of the sample. Several chabazite phases are indeed reported to unstable below  $\sim$ pH 2;<sup>41,42</sup> therefore, we ascribe this behavior to chabazite dissolution by the acidic lixiviant.

**Implications for Cementitious Environments.** Alkaline alteration of minerals by reaction with K-rich YCW solution will result in enhanced sorption potential with respect to cationic species such as  $\text{Sr}^{2+}$  either through increased adsorption to altered clay minerals and secondary intermediates or potential incorporation into newly formed phases.<sup>19,21</sup> At low temperatures (20–40 °C), K-chabazite supersaturation is predicted throughout the high pH reactions (Tables S4 and S5, Supporting Information) studied here (the K-feldspathoid mineral, leucite ( $\text{KAlSi}_2\text{O}_6$ ) was also predicted to be oversaturated; however, the degree of oversaturation was considerably lower than that of chabazite), but no crystalline phases form, and instead, an aluminosilicate gel occurred.<sup>5</sup> This is primarily due to the low temperature and high activation energies of crystallization (e.g.,  $>65$  kJ mol<sup>-1</sup> for zeolites<sup>43</sup>) that limit crystallization rates to very low levels. However, when reaction temperatures are elevated above 60 °C, several different zeolite phases are observed in K-rich YCW systems,<sup>15</sup> with K-chabazite the relevant phase at 60–70 °C.<sup>5</sup>

It is not known if the differences between the high- and low-temperature reaction end points simply reflect differences in crystallization rates or differences in mineral stabilities meaning that zeolite phases will not form at lower temperatures. However, when considering the transport of  $^{90}\text{Sr}$ , with a half-life of 29 years, even if zeolite phases were thermodynamically stable, the kinetics of crystallization may be slower than the few centuries required for  $^{90}\text{Sr}$  to decay to safe levels. Although the behavior of  $^{90}\text{Sr}$  is not relevant to geological disposal, it is interesting to note the preferential YCW reactions with reactive clay phases observed in these experiments. This is relevant to deep disposal where the results of this study and others<sup>19,21,23,36</sup> demonstrate it is reaction with clay mineral components of mineral assemblages that controls the development of solution chemistry and mineral surfaces.

In the systems without zeolite formation, the mineral surfaces present at high pH have a high sorption capacity for  $^{90}\text{Sr}$  due to changes to an inner-sphere adsorption mechanism in solutions with pH greater than 12–13. This indicates that very high pH ( $>12$ –13) will limit  $^{90}\text{Sr}$  transport at contaminated sites at all temperatures, where Sr can be susceptible to cation exchange by higher ionic strength ( $>10$  mmol L<sup>-1</sup>) waters.<sup>26</sup> It also suggests that any  $^{90}\text{Sr}$  associated with cement or concrete will not migrate a significant distance due to the highly alkaline nature of the cement pore fluids.

## ■ ASSOCIATED CONTENT

### 📄 Supporting Information

Detailed aqueous sampling and analysis methods; XAS methods; solid analysis methods; electron microprobe images and tabulated data; solution composition and mineral saturation modeling results; and SEM-EDX spectra. This material is available free of charge via the Internet at <http://pubs.acs.org>.

## ■ AUTHOR INFORMATION

### Corresponding Author

\*Phone: +44 113 3437532; fax: +44 113 3435259; e-mail: I.T. Burke@leeds.ac.uk.

### Notes

The authors declare no competing financial interest.

## ■ ACKNOWLEDGMENTS

The authors acknowledge funding from the U.K. Engineering and Physical Science Research Council and the U.K. Nuclear Decommissioning Authority (award 07000878). The European Synchrotron Radiation Facility is thanked for access to beamline BM26a (grant EC-740), and we acknowledge support from U.K. Natural Environment Research Council grant NE/H007768/1. We thank Rachel Gasior, Lesley Neve, and Richard Walshaw (University of Leeds) and Clare Thorpe (University of Manchester) for assistance with ICP-OES, XRD, electron microscopy, and XAS analysis, respectively.

## ■ REFERENCES

- (1) Fernandez, R.; Mader, U. K.; Rodriguez, M.; de la Villa, R. V.; Cuevas, J. Alteration of compacted bentonite by diffusion of highly alkaline solutions. *Eur. J. Mineral.* **2009**, *21* (4), 725–735.
- (2) Bickmore, B. R.; Nagy, K. L.; Young, J. S.; Drexler, J. W. Nitrate-cancrinite precipitation on quartz sand in simulated Hanford tank solutions. *Environ. Sci. Technol.* **2001**, *35* (22), 4481–4486.
- (3) Zhao, H. T.; Deng, Y. J.; Harsh, J. B.; Flury, M.; Boyle, J. S. Alteration of kaolinite to cancrinite and sodalite by simulated hanford tank waste and its impact on cesium retention. *Clays Clay Miner.* **2004**, *52* (1), 1–13.
- (4) Deng, Y. J.; Harsh, J. B.; Flury, M.; Young, J. S.; Boyle, J. S. Mineral formation during simulated leaks of Hanford waste tanks. *Appl. Geochem.* **2006**, *21* (8), 1392–1409.
- (5) Fernandez, R.; Rodriguez, M.; de la Villa, R. V.; Cuevas, J. Geochemical constraints on the stability of zeolites and C-S-H in the high pH reaction of bentonite. *Geochim. Cosmochim. Acta* **2010**, *74* (3), 890–906.
- (6) Khoury, H. N.; Salameh, E.; Clark, I. D.; Fritz, P.; Bajjali, W.; Milodowski, A. E.; Cave, M. R.; Alexander, W. R. A natural analogue of high pH cement pore waters from the Maqarin area of northern Jordan. I: Introduction to the site. *J. Geochem. Explor.* **1992**, *46* (1), 117–132.
- (7) Savage, D.; Walker, C.; Arthur, R.; Rochelle, C.; Oda, C.; Takase, H. Alteration of bentonite by hyperalkaline fluids: A review of the role of secondary minerals. *Phys. Chem. Earth, Parts A/B/C* **2007**, *32* (1–7), 287–297.
- (8) Ramirez, S.; Cuevas, J.; Vigil, R.; Leguey, S. Hydrothermal alteration of “La Serrata” bentonite (Almeria, Spain) by alkaline solutions. *Appl. Clay Sci.* **2002**, *21* (5–6), 257–269.
- (9) Nakayama, S.; Sakamoto, Y.; Yamaguchi, T.; Akai, M.; Tanaka, T.; Sato, T.; Iida, Y. Dissolution of montmorillonite in compacted bentonite by highly alkaline aqueous solutions and diffusivity of hydroxide ions. *Appl. Clay Sci.* **2004**, *27* (1–2), 53–65.
- (10) McKie, R. Sellafeld: The most hazardous place in Europe. *The Observer* [Online], April, 19, 2009. <http://www.guardian.co.uk/>

environment/2009/apr/19/sellafield-nuclear-plant-cumbria-hazards (accessed November 26, 2012).

(11) Barnes, M. C.; Addai-Mensah, J.; Gerson, A. R. The mechanism of the sodalite-to-cancrinite phase transformation in synthetic spent Bayer liquor. *Microporous Mesoporous Mater.* **1999**, *31* (3), 287–302.

(12) Deng, Y. J.; Flury, M.; Harsh, J. B.; Felmy, A. R.; Qafoku, O. Cancrinite and sodalite formation in the presence of cesium, potassium, magnesium, calcium and strontium in Hanford tank waste simulants. *Appl. Geochem.* **2006**, *21* (12), 2049–2063.

(13) Huang, W. L. The formation of illitic clays from kaolinite in KOH solution from 225°C to 350°C. *Clays Clay Miner.* **1993**, *41* (6), 645–654.

(14) Heller-Kallai, L.; Lapidés, I. Reactions of kaolinites and metakaolinites with NaOH—Comparison of different samples (Part 1). *Appl. Clay Sci.* **2007**, *35* (1–2), 99–107.

(15) Sanchez, L.; Cuevas, J.; Ramirez, S.; De Leon, D. R.; Fernandez, R.; Dela Villa, R. V.; Leguey, S. Reaction kinetics of FEBEX bentonite in hyperalkaline conditions resembling the cement-bentonite interface. *Appl. Clay Sci.* **2006**, *33* (2), 125–141.

(16) Savage, D. A review of analogues of alkaline alteration with regard to long-term barrier performance. *Mineral. Mag.* **2011**, *75* (4), 2401–2418.

(17) Gaucher, E. C.; Blanc, P. Cement/clay interactions – A review: Experiments, natural analogues, and modeling. *Waste Manage.* **2006**, *26* (7), 776–788.

(18) Chorover, J.; Choi, S. K.; Amistadi, M. K.; Karthikeyan, K. G.; Crosson, G.; Mueller, K. T. Linking cesium and strontium uptake to kaolinite weathering in simulated tank waste leachate. *Environ. Sci. Technol.* **2003**, *37* (10), 2200–2208.

(19) Chorover, J.; Choi, S.; Rotenberg, P.; Serne, R. J.; Rivera, N.; Strepka, C.; Thompson, A.; Mueller, K. T.; O'Day, P. A. Silicon control of strontium and cesium partitioning in hydroxide-weathered sediments. *Geochim. Cosmochim. Acta* **2008**, *72* (8), 2024–2047.

(20) Rod, K. A.; Um, W.; Flury, M. Transport of strontium and cesium in simulated Hanford tank waste leachate through quartz sand under saturated and unsaturated flow. *Environ. Sci. Technol.* **2010**, *44* (21), 8089–8094.

(21) Perdrial, N.; Rivera, N.; Thompson, A.; O'Day, P. A.; Chorover, J. Trace contaminant concentration affects mineral transformation and pollutant fate in hydroxide-weathered Hanford sediments. *J. Hazard. Mater.* **2011**, *197* (0), 119–127.

(22) Choi, S.; O'Day, P. A.; Rivera, N. A.; Mueller, K. T.; Vairavamurthy, M. A.; Seraphin, S.; Chorover, J. Strontium speciation during reaction of kaolinite with simulated tank-waste leachate: Bulk and microfocused EXAFS analysis. *Environ. Sci. Technol.* **2006**, *40* (8), 2608–2614.

(23) Thompson, A.; Steefel, C. I.; Perdrial, N.; Chorover, J. Contaminant desorption during long-term leaching of hydroxide-weathered Hanford sediments. *Environ. Sci. Technol.* **2010**, *44* (6), 1992–1997.

(24) Law, G. T. W.; Geissler, A.; Boothman, C.; Burke, I. T.; Livens, F. R.; Lloyd, J. R.; Morris, K. Role of nitrate in conditioning aquifer sediments for technetium bioreduction. *Environ. Sci. Technol.* **2010**, *44* (1), 150–155.

(25) Thorpe, C. L.; Lloyd, J. R.; Law, G. T. W.; Burke, I. T.; Shaw, S.; Bryan, N. D.; Morris, K. Strontium sorption and precipitation behaviour during bioreduction in nitrate impacted sediments. *Chem. Geol.* **2012**, *306–307*, 114–122.

(26) Wallace, S. H.; Shaw, S.; Morris, K.; Small, J. S.; Fuller, A. J.; Burke, I. T. Effect of groundwater pH and ionic strength on strontium sorption in aquifer sediments: Implications for <sup>90</sup>Sr mobility at contaminated nuclear sites. *Appl. Geochem.* **2012**, *27* (8), 1482–1491.

(27) Tessier, A.; Campbell, P. G. C.; Bisson, M. Sequential extraction procedure for the speciation of particulate trace-metals. *Anal. Chem.* **1979**, *51* (7), 844–851.

(28) Burke, I. T.; Livens, F. R.; Lloyd, J. R.; Brown, A. P.; Law, G. T. W.; McBeth, J. M.; Ellis, B. L.; Lawson, R. S.; Morris, K. The fate of technetium in reduced estuarine sediments: Combining direct and indirect analyses. *Appl. Geochem.* **2010**, *25* (2), 233–241.

(29) Tenderholt, A.; Hedman, B.; Hodgson, K. O. PySpline: A modern, cross-platform program for the processing of raw averaged XAS edge and EXAFS data. *AIP Conf. Proc.* **2007**, *882*, 105–107.

(30) Tomic, S.; Searle, B. G.; Wander, A.; Harrison, N. M.; Dent, A. J.; Mosselmans, J. F. W.; Inglesfield, J. E. *New Tools for the Analysis of EXAFS: The DL\_EXCURV Package*, CCLRC Technical Report DL-TR-2005-00, ISSN 1362-0207; Daresbury Synchrotron Radiation Source: Cheshire, England, 2005.

(31) Gurman, S. J.; Binsted, N.; Ross, I. A rapid, exact curved-wave theory for EXAFS calculations. *J. Phys. C: Solid State Phys.* **1984**, *17* (1), 143–151.

(32) Binsted, N.; Strange, R. W.; Hasnain, S. S. Constrained and restrained refinement in EXAFS data analysis with curved wave theory. *Biochemistry* **1992**, *31*, 12117–12125.

(33) Nikitenko, S.; Beale, A. M.; van der Eerden, A. M. J.; Jacques, S. D. M.; Leynaud, O.; O'Brien, M. G.; Detollenaere, D.; Kaptein, R.; Weckhuysen, B. M.; Bras, W. Implementation of a combined SAXS/WAXS/QEXAFS set-up for time-resolved in situ experiments. *J. Synchrotron Radiat.* **2008**, *15*, 632–640.

(34) Qafoku, N. P.; Ainsworth, C. C.; Szecsody, J. E.; Qafoku, O. S. Aluminum effect on dissolution and precipitation under hyperalkaline conditions: I. Liquid phase transformations. *J. Environ. Qual.* **2003**, *32* (6), 2354–2363.

(35) Krauskopf, K. B.; Bird, D. K. *Introduction to Geochemistry*, 3rd ed.; McGraw-Hill: New York, 1995.

(36) Qafoku, N. P.; Ainsworth, C. C.; Szecsody, J. E.; Bish, D. L.; Young, J. S.; McCready, D. E.; Qafoku, O. S. Aluminum effect on dissolution and precipitation under hyperalkaline conditions: II. Solid phase transformations. *J. Environ. Qual.* **2003**, *32* (6), 2364–2372.

(37) Calligaris, M.; Nardin, G.; Randaccio, L.; Chiaramonti, P. C. Cation-site location in a natural chabazite. *Acta Crystallogr., Sect. B: Struct. Sci.* **1982**, *38* (FEB), 602–605.

(38) Ahmed, I. A. M.; Young, S. D.; Mosselmans, J. F. W.; Crout, N. M. J.; Bailey, E. H. Coordination of Cd<sup>2+</sup> ions in the internal pore system of zeolite-X: A combined EXAFS and isotopic exchange study. *Geochim. Cosmochim. Acta* **2009**, *73* (6), 1577–1587.

(39) Lide, D. R. *CRC Handbook of Chemistry and Physics*, 88th ed.; CRC Press, Taylor & Francis Group: Boca Raton, FL, 2007.

(40) Dang, L. X.; Schenter, G. K.; Fulton, J. L. EXAFS spectra of the dilute solutions of Ca<sup>2+</sup> and Sr<sup>2+</sup> in water and methanol. *J. Phys. Chem. B* **2003**, *107* (50), 14119–14123.

(41) Hasegawa, Y.; Hotta, H.; Sato, K.; Nagase, T.; Mizukami, F. Preparation of novel chabazite (CHA)-type zeolite layer on porous α-Al<sub>2</sub>O<sub>3</sub> tube using template-free solution. *J. Membr. Sci.* **2010**, *347* (1–2), 193–196.

(42) Mimura, H.; Kanno, T. Distribution and fixation of cesium and strontium in zeolite A and chabazite. *J. Nucl. Sci. Technol.* **1985**, *22* (4), 284–291.

(43) Yang, S.; Navrotsky, A. An in situ calorimetric study of zeolite crystallization kinetics. *Microporous Mesoporous Mater.* **2002**, *52* (2), 93–103.